

## Front-light Structure with Excitation Light Polarized for Enhancing Lensless Fluorescence Imaging

Arphorn Promking,<sup>1</sup> Yoshinori Sunaga,<sup>2</sup> Yasumi Ohta,<sup>2</sup>  
Ryoma Okada,<sup>1,3</sup> Hironari Takehara,<sup>1,4</sup> Makito Haruta,<sup>2,5</sup>  
Hiroyuki Tashiro,<sup>1,6</sup> Jun Ohta,<sup>2</sup> and Kiyotaka Sasagawa<sup>1,3\*</sup>

<sup>1</sup>Division of Materials Science, Graduate School of Science and Technology,  
Nara Institute of Science and Technology, 8916-5 Takayama, Ikoma, Nara 630-0192, Japan

<sup>2</sup>Institute for Research Initiatives, Nara Institute of Science and Technology,  
8916-5, Takayama, Ikoma, Nara 630-0192, Japan

<sup>3</sup>Medilux Research Center, Nara Institute of Science and Technology,  
8916-5, Takayama, Ikoma, Nara 630-0192, Japan

<sup>4</sup>Nara Advanced Imaging Technology, Co., Ltd., 8916-12, Takayama, Ikoma, Nara 630-0101, Japan

<sup>5</sup>Department of Opto-Electronic System Engineering, Faculty of Science and Engineering,  
Chitose Institute of Science and Technology, 758-65 Bibi, Chitose, Hokkaido 066-8655, Japan

<sup>6</sup>Department of Health Sciences, Faculty of Medical Sciences, Kyushu University,  
3-1-1 Maidashi, Higashi-ku, Fukuoka 812-8582, Japan

(Received February 12, 2025; accepted March 12, 2025)

**Keywords:** lensless imaging device, fluorescent imaging, front-light structure, diffractor, light-polarized

In this study, we introduce a high-performance front-light structure integrated with optical polarization control to improve low-contrast fluorescent imaging in lensless devices. Lensless fluorescence imaging is an advanced technology with the potential to enhance the performance of biological and neurological imaging. However, there are still challenges to achieving high image quality, particularly in low-contrast fluorescent signals due to light scattering and absorption. The performance of a low-fluorescence stripe diffractor, fabricated using Norland Optical Adhesive 63 (NOA 63), was evaluated in comparison to polydimethylsiloxane (PDMS) material as a light guide. The diffractor is designed to operate with a hybrid emission filter on the image sensor. As a result, by coupling a 450 nm laser with either P- or S-polarization, it was shown that NOA 63 is notable as a diffractor material. Notably, S-polarized light showed a great excitation intensity and an enhanced contrast in fluorescent bead imaging compared with P-polarized light. Furthermore, the system was validated for biological applications by successfully detecting fluorescent bead emission in agarose-embedded samples of various thicknesses, simulating brain tissue. These results emphasize the system's ability to capture low-intensity fluorescence signals from deep layers of biological tissue.

---

\*Corresponding author: e-mail: [sasagawa@ms.naist.jp](mailto:sasagawa@ms.naist.jp)  
<https://doi.org/10.18494/SAM5600>

## 1. Introduction

Lensless fluorescent imaging, with its recent advancements, has emerged as a powerful alternative to traditional fluorescence microscopy, with promising tools for cellular studies, large field-of-view (FOV) imaging, and dynamic biological imaging.<sup>(1–4)</sup> Conventional fluorescent imaging systems, while capable of achieving high spatial resolution, are limited by a restricted FOV due to the physical constraints of lenses and optical paths. Additionally, these systems typically require the immobilization of specimens or the restraint of animals, hindering the investigation of freely moving behavior.<sup>(5–7)</sup> On the other hand, lensless fluorescent imaging overcomes these limitations by eliminating bulky optical components and directly capturing fluorescent light on a sensor. This approach results in a compact, lightweight design well-suited for studies involving freely behaving organisms,<sup>(8)</sup> particularly observing dynamic brain activity in neuroscience. Head-mounted fluorescence microscopes without optical lens components have been used successfully to monitor brain activity with unrestrained movement.<sup>(9,10)</sup> However, heavy and cumbersome devices attached to the head can restrict an animal's ability to navigate its environment. Building on this concept, we developed a novel implantable fluorescence imaging device with a lensless structure. This device enables the observation of specific neural regions within the deep mouse brain while allowing for free movement.<sup>(11,12)</sup>

Despite these advancements, lensless fluorescence imaging devices have been facing challenges in light collection performance. Their compact and resource-constrained designs can result in reduced spatial resolution and low signal-to-noise ratios (SNRs). Emission filters, including absorption filters, are generally integrated into the image sensor to block unwanted light,<sup>(13,14)</sup> whereas interference filters are designed to either reflect or transmit specific spectral wavelengths of interference.<sup>(15,16)</sup> However, the effectiveness of these filters is often insufficient, particularly in areas with dense biological activity.<sup>(17)</sup> Recently, we have proposed a hybrid filter, which is a complementary combination of interference and absorption filters with a fiber-optic plate (FOP) integrated into a single structure. This design enabled the rejection of high-excitation light while effectively improving resolution in lensless fluorescent imaging, such as the green fluorescent protein of mouse brain slices.<sup>(18,19)</sup> Moreover, we are committed to enhancing the capabilities of our implantable fluorescence imaging device to facilitate the observation of neural processes within the deep brain. We have successfully demonstrated the operation of the hybrid filter with a front-light structure to achieve epifluorescence imaging in lensless image devices. The result shows promise in improving image contrast.<sup>(20)</sup>

The front-light structure is designed as a waveguide, with the hybrid filter reflecting the excitation light and delivering it uniformly to the fluorescent samples while transmitting the emission light to a lensless imaging device. However, the performance of the front-light system in previous studies<sup>(20)</sup> still needs consideration, as shown in Fig. 1. A high autofluorescence from the characteristics of a diffractor material placed between the image sensor's pixel array and the imaged sample was observed. This autofluorescence may obscure the emitted fluorescence signal, particularly in weak fluorescent samples. Additionally, the increased thickness of the glass light guide has extended the observation distance, which has led to a degradation in image resolution. Moreover, the unstable light power propagation and imperfect

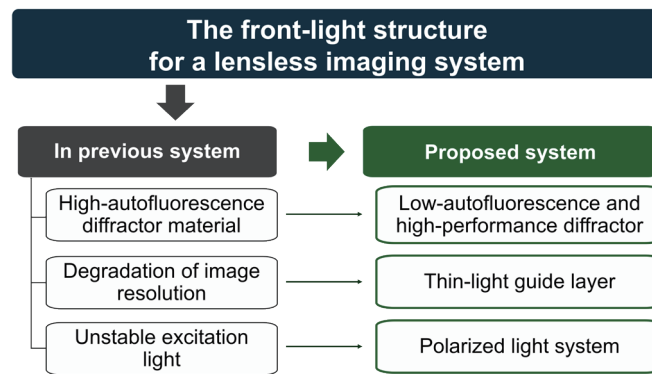


Fig. 1. (Color online) Diagram of proposed technical solution of front-light structure for lensless imaging system.

polarization of the excitation light within the waveguide have posed challenges, affecting the consistency and effectiveness of the front-light structure.

Therefore, in this study, we proposed a new front-light structure designed to minimize autofluorescence and enhance the effectiveness of lensless fluorescence imaging using a polarized excitation light system. We considered commonly used materials in microfabrication, including SU-8, Norland Optical Adhesive 63 (NOA 63), and polydimethylsiloxane (PDMS) as diffractors,<sup>(21,22)</sup> which not only exhibit low fluorescence but also allow for a suitable fabrication process. The front-light structure was fabricated with a stripe pattern on a thin cover glass by imprinting photography. Our lensless fluorescence imaging system uses a 450 nm laser fiber as excitation light, controlled in both the P- and S-polarized directions before being coupled with the light guide. As a result, initial experiments identified NOA 63 as the optimal diffractor material for our front-light structure, as it exhibits a strong excitation light profile in a fluorescein solution. We then validated and optimized the proposed system by evaluating the intensity of microsphere beads and assessing its effectiveness through scattering simulations of brain tissue using different agarose gel thicknesses to model the scattering properties.

## 2. Data, Materials, and Methods

### 2.1 Overall concept of front-light structure

The proposed front-light structure with an excitation light polarized system for lensless fluorescent imaging, along with a cross section of light propagation, is illustrated in Fig. 2. This concept realizes epifluorescence imaging. A low-autofluorescence diffractor was fabricated on a thin cover glass, which acts as a light guide. This diffractor is positioned to operate with a high-performance hybrid filter located above the imaging sensor. Owing to the light guide's and stripe diffractor's close refractive indices, the blue excitation light can transmit into the interference filter and be rejected by reflecting toward the observation target. The hybrid filter structure was used in the same way as in a previous study.<sup>(19)</sup> This filter, as shown in Fig. 2, is composed of an interference filter with a short pass at 560 nm (pink layer), which is separated by an FOP, and a

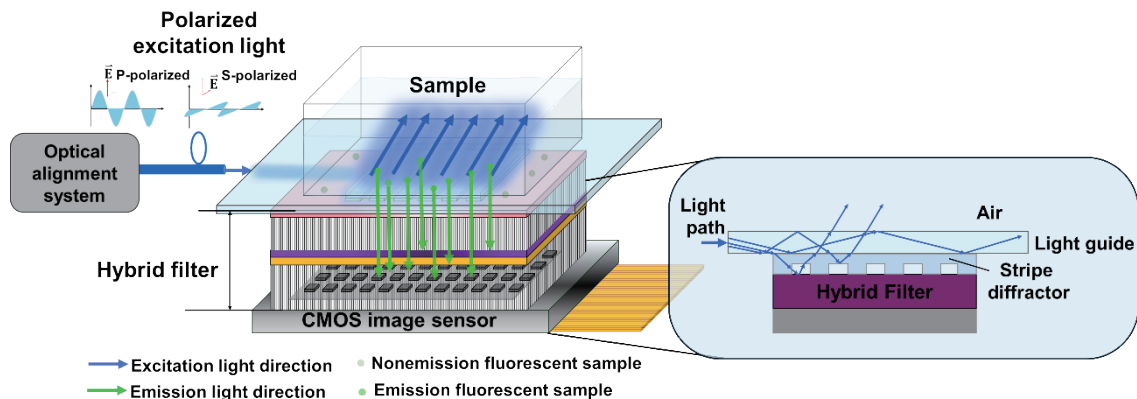


Fig. 2. (Color online) Proposed front-light structure with optical polarization in lensless imaging device and cross section of excitation light propagation within front-light structure.

filter with a long pass at 490 nm (purple layer). It is bonded to an absorption filter (yellow layer), which is coated onto another FOP in front of the image sensor. This design effectively transmits green fluorescent light while efficiently rejecting blue excitation light. Finally, the optical alignment system has been set up to control the polarized light direction of the excitation light fiber before coupling into one side of the diffractor substrate. The fluorescent sample is placed atop the proposed front-light structure and imaged using a CMOS image sensor from the bottom. This approach is expected to improve light propagation within the front-light structure, resulting in substantial emissions from the target using an implantable fluorescence imaging device.

## 2.2 Diffractor fabrication

Sasagawa *et al.*<sup>(20)</sup> reported that the SU-8 negative photoresist (SU-8 3010, Kayaku Advanced Materials) stripe diffractor showed very high fluorescence, which tends to obscure an emitted fluorescence signal, especially a weak signal. Here, the performance characteristics of common materials widely used for microfluidic devices compatible with microfabrication, transparency, and low autofluorescence, such as NOA 63 (Norland Products Inc.) and PDMS (KE-106/CAT-RG, Shin-Etsu silicone), were compared to choose one that most matches our application. The SU-8 diffractor pattern was fabricated as a mold by photolithography and transferred with NOA 63 and PDMS by imprinting. The cleaned cover-glass substrate of 150  $\mu\text{m}$  thickness was spin-coated with SU-8 and then exposed to UV light through a stripe photomask at 100  $\text{mJ}/\text{cm}^2$  for 11 s to make a pattern on SU-8. At the end of the process, the mold achieved a thickness of 10  $\mu\text{m}$  and a pitch of 90  $\mu\text{m}$ . These dimensions were measured using a digital microscope (VHX-7100 with objective lens VHX-E100), as shown in Fig. 3, revealing both the top and cross-sectional side views of the stripe pattern. The pitch design has been evaluated for the final mounting of our implantable micro-image sensor device. The pixel pitch of the image sensor is 15  $\mu\text{m}$ , with each pixel measuring 7.5  $\mu\text{m}$ . In comparison, each pitch of the diffractor is six times larger, ensuring a comprehensive coverage of the image sensor array, which has a resolution of  $120 \times 268$  pixels.

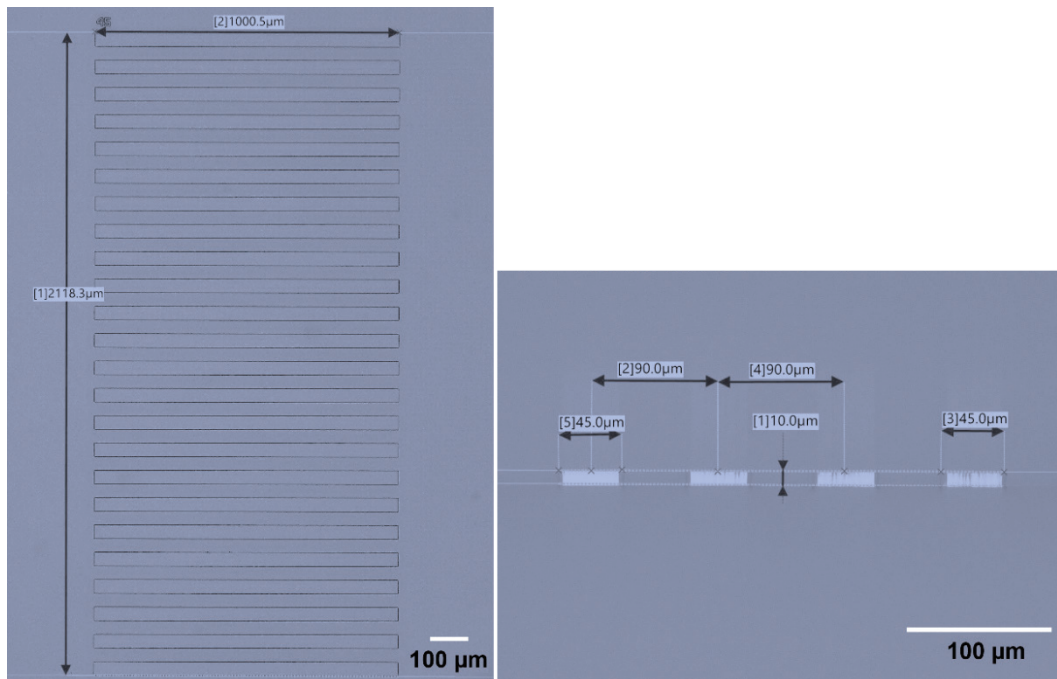


Fig. 3. (Color online) SU-8 diffractor mold with top and cross-sectional side views of stripe pattern measured using digital microscope.

An imprinting process utilizing NOA 63 and PDMS is illustrated in Fig. 4, where the SU-8 mold is spin-coated with 1% of an amorphous perfluorinated polymer, CYTOP type A, to form a protective bonding layer. Figure 4(a) shows the process for the NOA 63 diffractor. A small amount of NOA 63 was applied directly to the SU-8 pattern mold and covered with a 30- $\mu\text{m}$ -thick cover glass (D263T, Matsunami Glass Ind., Ltd.). During this step, gentle pressure is applied to dispense a thin NOA 63 layer and avoid air bubbles within the diffractor area. The assembly was exposed to UV light for 30 s, followed by demolding by carefully separating the cured NOA 63 from the mold. We used a thin cover glass as a light guide to enhance the light propagation loss. Therefore, owing to the slight refractive index mismatch between the glass ( $\approx 1.5$ ) and PDMS ( $\approx 1.4$ ), light's bending will occur at the interface according to Snell's Law, and the reflection and transmission of light will be affected by the Fresnel equations. Two processes used to make a PDMS diffractor are considered. For PDMS imprinting on the glass, as shown in Fig. 4(b), the PDMS was prepared with a 10:1 ratio and by pattern imprinting, the same as the NOA 63 processes except that, in step (ii), the PDMS was cured at a temperature of 150  $^{\circ}\text{C}$  on a hot plate for 30 min. For imprinting with PDMS only shown in Fig. 4(c), we intended to achieve a small thickness while keeping the shape consistent; thus, the PDMS was prepared with a 6:1 ratio. Liquid PDMS (0.5 ml) was dropped using a syringe and spin-coated to achieve a small thickness on the SU-8 mold. After it was cured at 150  $^{\circ}\text{C}$ , it was peeled off from the mold. In our experiment, the amounts of NOA 63 and PDMS applied to the mold and the pressure to dispense could not be controlled consistently, causing the diffractor's dimensions to shift slightly. Therefore, the three samples for each process were fabricated to obtain the average

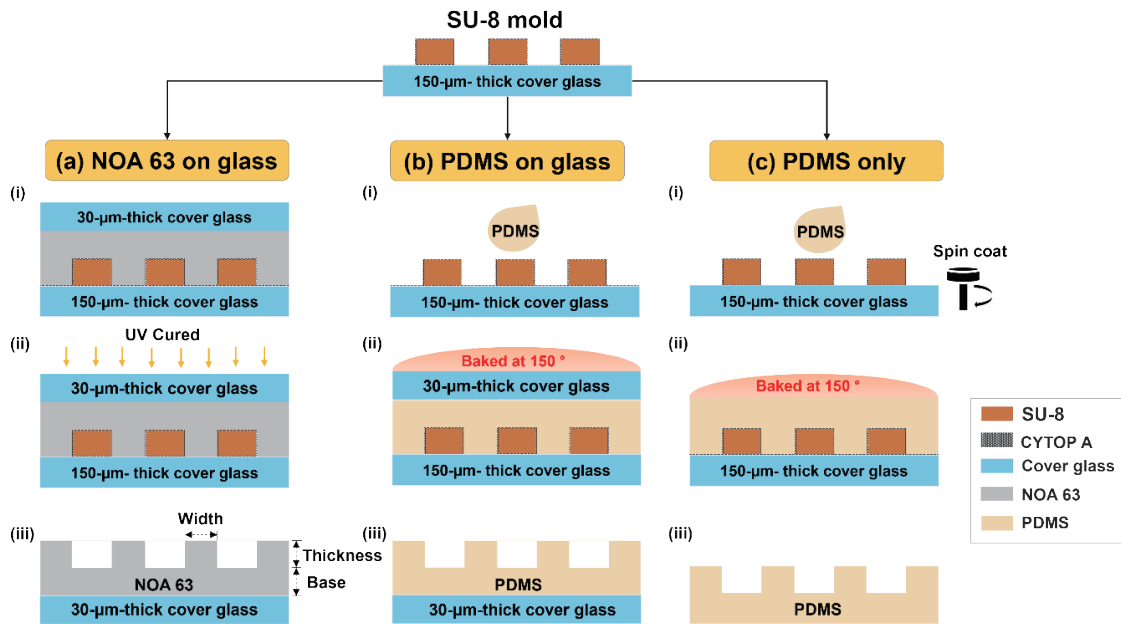


Fig. 4. (Color online) Imprinting processes for transferring SU-8 mold with (a) NOA 63 on thin cover glass, (b) PDMS on thin cover glass, and (c) PDMS only.

dimensions consisting of the height (thickness + base) and width. For the NOA 63 diffractor, we achieved a height of around 15  $\mu\text{m}$  and a width of 44.6  $\mu\text{m}$ . In the case of the PDMS pattern on a cover glass, the height was 12  $\mu\text{m}$  and the width was 44.8  $\mu\text{m}$ . The smallest height that we can handle for imprinting with PDMS only was 70  $\mu\text{m}$  and the width was 45.7  $\mu\text{m}$ .

### 2.3 Polarized excitation light system

The polarization of light is a property of light that describes the orientation of the electric field vector ( $\vec{E}$ ) oscillations. Random polarization orientation can affect performance, whether in the front-light structure or the interference filter, which can affect reproducibility. In this study, we proposed a polarized excitation light system to enhance the performance of the lensless imaging system with the front-light structure, which is shown in the setup system in Fig. 5(a) and a schematic system in Fig. 5(b). A thermoelectrically cooled laser diode mount (TCLDM9, Thorlabs) with a laser diode of 450 nm wavelength was used as the excitation light. The light is transmitted through the single-mode fiber (SMF, P5-405B-PCAPC-1, Thorlabs) and in a polarized state to achieve linear polarization using a two-paddle fiber polarization controller (FPC021 Thorlabs). The linear polarization was ensured by examining the angle of the polarizer versus the power output to show a sinusoidal pattern over a 360° rotation. Both orientations, P- and S-polarizations, were investigated and defined by an orientation of  $\vec{E}$  to the plane of incidence (POI) at a light wave interacting with a surface. For P-polarization, the  $\vec{E}$  direction is parallel to POI, whereas for S-polarization, the  $\vec{E}$  direction is perpendicular to POI. In this study, POI is considered vertical at the boundary between the light guide and the diffractor pattern.

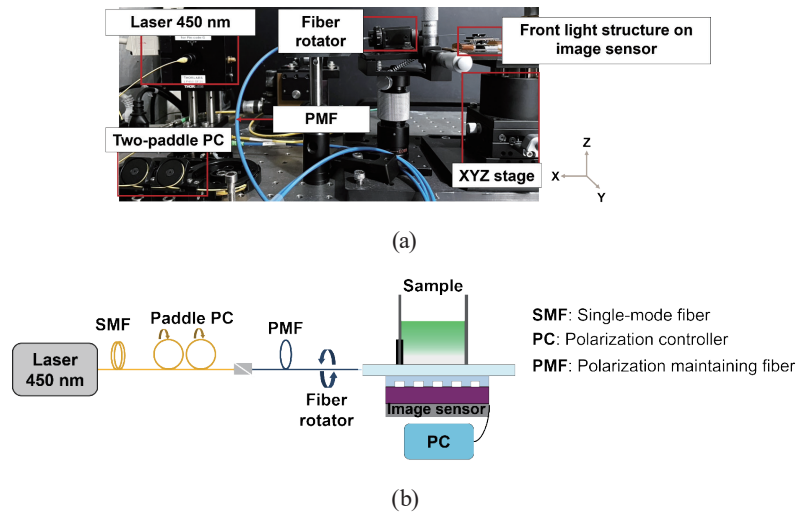


Fig. 5. (Color online) (a) Polarized excitation light system and (b) control schematic of polarized excitation light coupled to proposed front light in lensless fluorescent imaging device.

The linearly polarized light was connected to a polarization-maintaining fiber optic (PMF, P3-405BPM-FC-2, Thorlabs) to maintain the light state. The direction of the orientation was controlled by a fiber rotator before coupling to a glass substrate. The P- or S-polarized light was coupled to the cover glass using the butt-joint technique. A commercial image sensor (STC-MCS231U3V, Omron Sentech) removed a glass lid in front of the image pixels using a Nd: YAG laser and bonded a hybrid filter structure to its surface to image the contrast of the fluorescent sample. The image is monitored on imaging software. Additionally, as the fiber optic and glass were not secured with adhesive, the assembly of image sensors was fixed onto the *XY*-axis translation stage (TSD-602C, OptoSigma) equipped with the *Z*-axis translation stage (TSD-601SZ, OptoSigma) to adjust the sample position.

## 2.4 Fluorescent sample preparation

A small cuvette was prepared to contain a sample consisting of the fluorescein solution, microsphere bead, and simulated agarose tissue. The bottom of the cuvette was trimmed and a thin layer of NOA 63 was applied to its rim. The cuvette was then securely attached to the cover glass of NOA 63 by PDMS diffractor imprinting, where a thin layer of NOA 63 formed a strong adhesive after curing with UV light. For the PDMS only diffractor, a PDMS liquid was applied to the cuvette rim and heated to achieve adhesiveness. Moreover, to prevent light interference from the affixed areas, the black resist was applied around the front region of the cuvette, as well as along the boundary between the cuvette and the glass or PDMS substrate.

- Fluorescein solution and microsphere beads

Sodium fluorescein (Uranine, 213-00092, FUJIFILM Wako Pure Chemical) was diluted with deionized water (DIW) to a concentration of 0.133  $\mu\text{mol/L}$  to obtain a fluorescein solution. To obtain a microsphere solution, FluoSpheres (15  $\mu\text{m}$  in size, F8844, ThermoFisher) were diluted in DIW at 1:100 dilution.

- Preparation of simulated tissue using agarose

A 1% agarose solution was prepared and mixed with microsphere beads to simulate brain tissue. To make the solution, agar powder (018-15811, FUJIFILM Wako Pure Chemical) was added to DIW and heated in a microwave until fully dissolved. The solution was then allowed to cool to 55 °C on a hot plate. Once cooled, 5 mL of the solution was poured into a small petri dish, and 30  $\mu$ L of 15- $\mu$ m-diameter microsphere beads was added and gently mixed and then allowed to solidify. Finally, the solidified gel was sliced into 50, 100, and 200  $\mu$ m sections using a slicer (LinearSlicer PR07, DOSAKA EM CO) and immersed in DIW.

### 3. Experimental Results

#### 3.1 Comparison of autofluorescence values from diffractor materials

The SU-8 mold, NOA 63, and PDMS diffractors were examined for fluorescence using a fluorescence microscope (M165FC, Leica), the setup measurement system shown in Fig. 6(a). A custom stand was designed to securely hold the samples during imaging. Blue excitation light (450–490 nm) was directed onto the top of each sample, and the emitted fluorescence was captured from above using a 30 ms exposure time. The comparison of autofluorescence

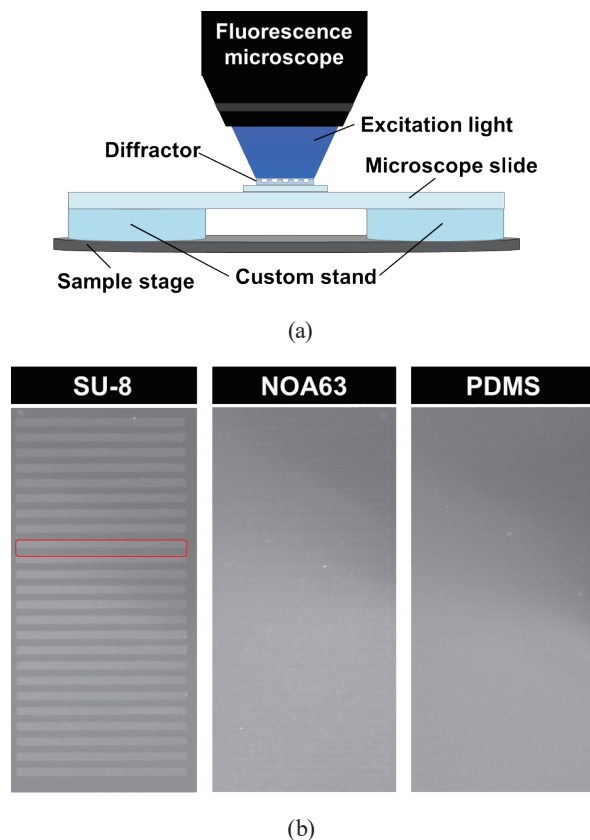


Fig. 6. (a) Autofluorescence measurement system. (b) Autofluorescence results of SU-8, NOA 63, and PDMS diffractors.

materials is shown in Fig. 6(b). The SU-8 stripes exhibited clear fluorescence compared with the surrounding glass substrate, whereas the NOA 63 and PDMS patterns demonstrated very low fluorescence. We randomly calculated the difference in average light intensity between the stripe pattern and the background by choosing a representative in the red rectangle for all materials. The values obtained were 12.3 for SU-8, 3.3 for NOA63, and 1.6 for PDMS. Notably, the PDMS exhibited slightly lower fluorescence than did NOA 63 that was also noticeable to the naked eye.

### 3.2 Irradiated pattern of the excitation light from the front-light structure

The intensity profile of excitation light in fluorescein solutions was observed to evaluate the effectiveness of the diffractor material and the fabrication process in irradiating light in front of lensless image sensors. The fluorescein solution was dropped into the cuvette of the diffractor sample, which was then placed stably on the hybrid filter layers of the image sensor. The excitation light power for all experiments in this study was set to 4 mW. During this experiment, as the image sensor was located under the sample, we used image software to monitor the specific area to ensure that all conditions, such as the placement position, were consistent for result comparison. In the proposed imaging system, the P- and S-polarized excitation lights are switched by changing the angle of the rotator. The *X*-axis translation was used to keep a glass or PDMS substrate close to the fiber core and achieve a position of high excitation light intensity by adjusting the *YZ* axis. The irradiated profile of excitation light from the front-light structure for each diffractor sample is shown in Fig. 7(a) based on observation. We found that the light-profile refraction with P- and S-polarized lights in the water had occurred on NOA 63 and the PDMS only diffractor, whereas no distinct light profile was observed in the PDMS diffractor on glass. This is probably a result of the total internal reflection (TIR) in the glass due to the reflective index mismatch between glass and PDMS. Although the PDMS only diffractor enhanced excitation intensity, we also noted the multimode propagation of light along the optical path. Multimode propagation happens when light travels along several paths within a material, leading to dispersion and mode interference. This was attributed to the properties of PDMS, which are being soft and flexible, and low reflective index homogeneity, causing the excitation light to scatter in multiple directions and resulting in intensity fluctuations within the diffractor area and its surrounding. In contrast, NOA 63, despite exhibiting a slightly higher autofluorescence than PDMS, demonstrated a stronger beam profile and a higher excitation light intensity. Owing to its rigidity characteristics, as observed in this result, the NOA 63 diffractor is well suited for our system.<sup>(23)</sup>

Subsequently, the excitation light intensity within the NOA 63 pattern was analyzed to examine the effective configuration between P- and S-polarized lights. While observing the light beam profile in water, we collected the intensity distribution of the excitation light within the pattern using our proposed imaging system with a 500 ms exposure time. The results are shown in Fig. 7(b), with the full width at half maximum (FWHM) in the diffractor region plotted in Fig. 7(c). From the graph, S-polarized excitation light provided a wider excitation area, resulting in a larger FWHM and also a slightly higher excitation intensity than P-polarized light.

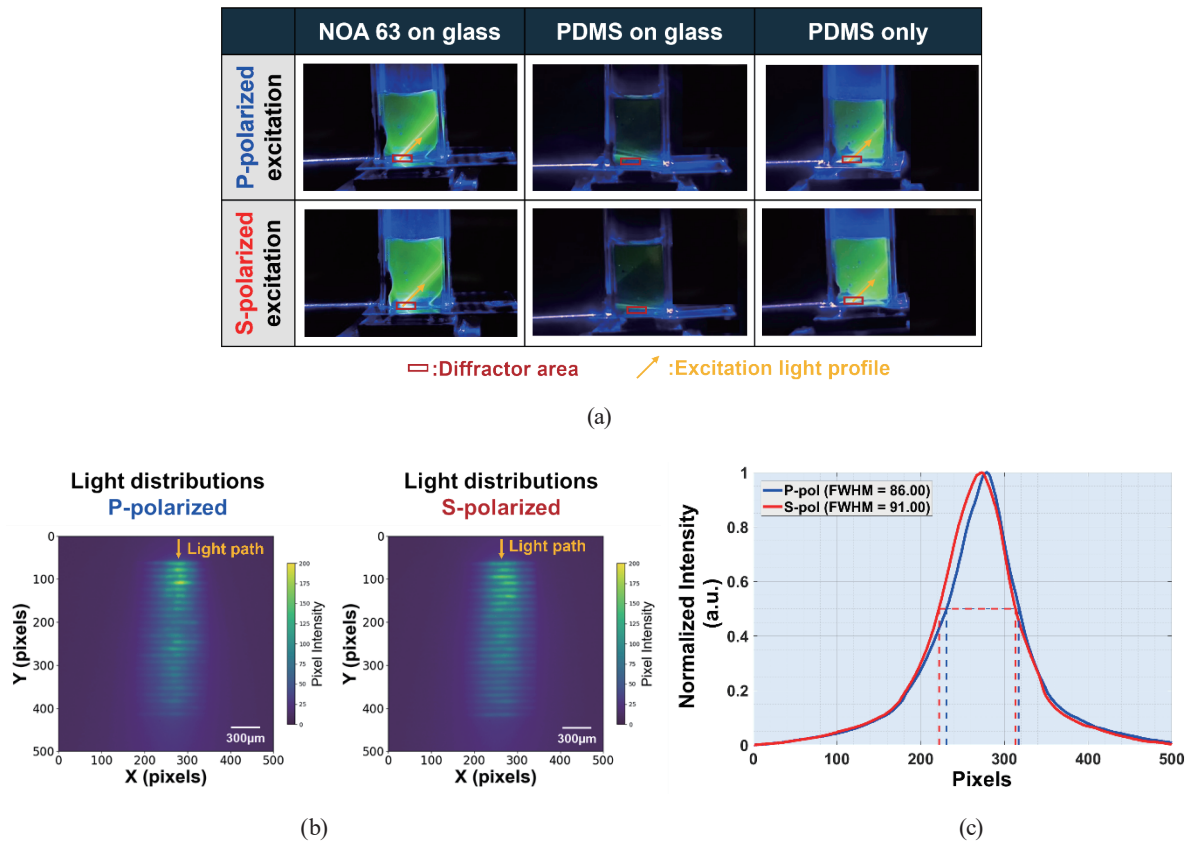


Fig. 7. (Color online) (a) Excitation light profile with P- and S-polarizations in fluorescein of NOA 63 pattern on glass, PDMS pattern on glass, and PDMS only pattern. (b) Intensity distribution of excitation light within pattern and (c) FWHM in diffractor region.

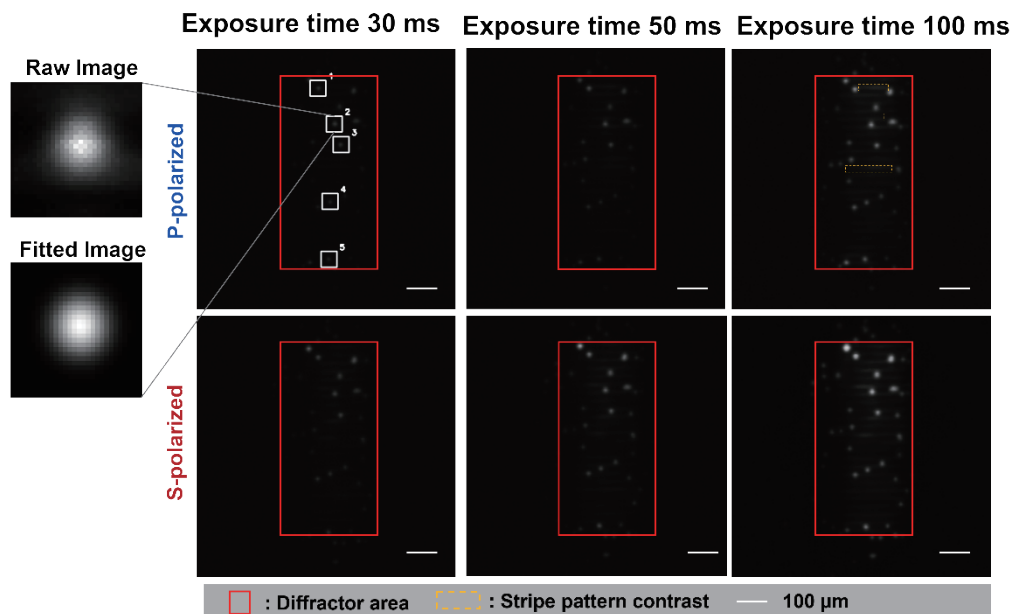
The average non-normalized light intensity within the peak intensity FWHM basis was obtained, with 55 grayscale values for P-polarized light and 60 grayscale values for S-polarized light. This suggests that S-polarized light can enhance the image contrast in our system. However, an uneven distribution of light was observed, with a high-intensity region at the beginning of the pattern (from pixels 50 to 200 on the Y-axis), gradually decreasing toward the end. This variation is expected owing to optical losses during light propagation, which will also affect the fluorescence observed in the sample.

### 3.3 Effect of polarized excitation light on the front-light structure with fluorescent beads

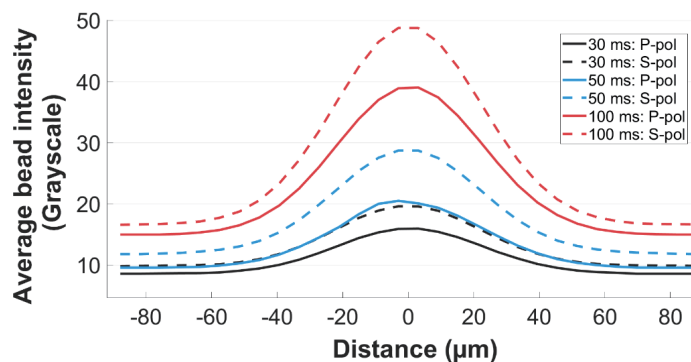
The front-light structure with low fluorescence, i.e., the NOA 63 diffractor, was confirmed to have strong irradiated excitation light in front of lensless image sensors. Here, the fluorescent bead imaging was conducted to validate and optimize the effectiveness of the front-light structure with the polarized light system. In a lensless imaging system, selecting the proper exposure time is crucial for image quality. Too short an exposure causes noisy, underexposed images, whereas too long an exposure leads to saturation and loss of detail. Moreover, it is essential to consider the effect of diffractor patterns from the front-light structure, as improper

settings can blur the delicate features of observed targets. Therefore, we determined the optimal exposure time for the proposed image system by comparing the intensities of the fluorescent beads.

A 15- $\mu\text{m}$ -diameter fluorescent bead solution was added to the cuvette of the NOA 63 diffractor instead of fluorescein water, and a bead was allowed to settle at the diffractor position for 20 min. The exposure time was set to 30, 50, and 100 ms, and the fluorescent bead images were captured in both P- and S-polarized lights. The result is shown in Fig. 8(a), revealing that the effect of the front-light structure coupling with P- and S-polarized lights can enhance the increasing intensity of fluorescent beads.



(a)



(b)

Fig. 8. (Color online) Optimizing performance of front-light structure with P- and S-polarizations on fluorescent beads: (a) intensity of fluorescent beads within NOA 63 diffractor region at exposure times of 30, 50, and 100 ms, and (b) comparison graph of average bead intensities in diffractor area from five beads at different exposure times.

To evaluate the intensity, five bead representatives were selected from each exposure time in both polarization results, such as the image from P-polarized light at an exposure time of 30 ms. Each raw bead image was fitted to a 2D Gaussian function for an accurate intensity profile, such as bead 2 in P-polarized light at an exposure time of 30 ms. The intensities of the representative beads were then averaged and compared, as shown in Fig. 8(b). As a result, the measured light intensity increased linearly according to exposure time for both P- and S-polarized lights. In particular, the average bead intensity from S-polarized light is shown to be higher, which agrees with the result of the light intensity distribution in the diffractor region. Although the 100 ms exposure time yielded a higher bead contrast image than the 30 ms exposure time, it also produced a notable stripe pattern. This effect can be seen in the region of P-polarized light indicated by the yellow dashed line in Fig. 8(a), as well as in the corresponding areas of S-polarized light, which are clearly observed. Given the low emission from live cells, this high-intensity pattern can obscure important details. To balance high intensity and reduced pattern visibility, we chose an exposure time of 50 ms while maintaining S-polarized light for our fluorescent imaging system. Additionally, five fitted beads under these parameters were calculated using the FWHM to determine the resolution of the acquired image, which is approximately 50  $\mu\text{m}$  in our current system.

### 3.4 Brain tissue simulation using agarose gel

We evaluated the performance of our proposed system in detecting fluorescent signals within agarose gel slices of various thicknesses, simulating brain tissue conditions. Agarose gel exhibits optical scattering properties that mimic the light-scattering behavior of brain tissue, whereas microsphere beads act as point-like fluorescent sources to simulate targets of interest. The 50 and 100  $\mu\text{m}$  samples represent thin tissue-like conditions, whereas the 200  $\mu\text{m}$  gel simulates moderate thickness. The measurement system for brain tissue simulation is shown in Fig. 9(a). Agarose gel slices mixed with microsphere beads were carefully placed in a cuvette containing a small amount of DIW to prevent drying. Bead intensity images were captured from the bottom using our lensless imaging system, and we confirmed the bead positions and intensities within the diffractor area from the top using a fluorescence microscope. Both systems were configured with a 50 ms exposure time. As shown in Fig. 9(b), our lensless system, which incorporated a low-fluorescence front-light structure with S-polarized excitation light, effectively detects emission signals from fluorescent beads in gels of increasing thickness. As expected, the intensity of the fluorescent beads decreased with increasing gel thickness.

More interestingly, despite the overall decrease in intensity with a thicker gel, we observed an uneven distribution of bead intensity within the same thickness from our imaging system. It was assumed that beads located deeper from the detector exhibited significantly lower fluorescence intensity. This is supported by the results shown in Fig. 9(c), which compares the intensities of three selected beads from each gel thickness between our proposed system and a standard fluorescence microscope. The intensities were determined on the basis of the peak intensity FWHM of each bead, and their average was calculated. Since both systems capture images from opposite sides, beads positioned deeper in the gel showed a higher intensity in our lensless

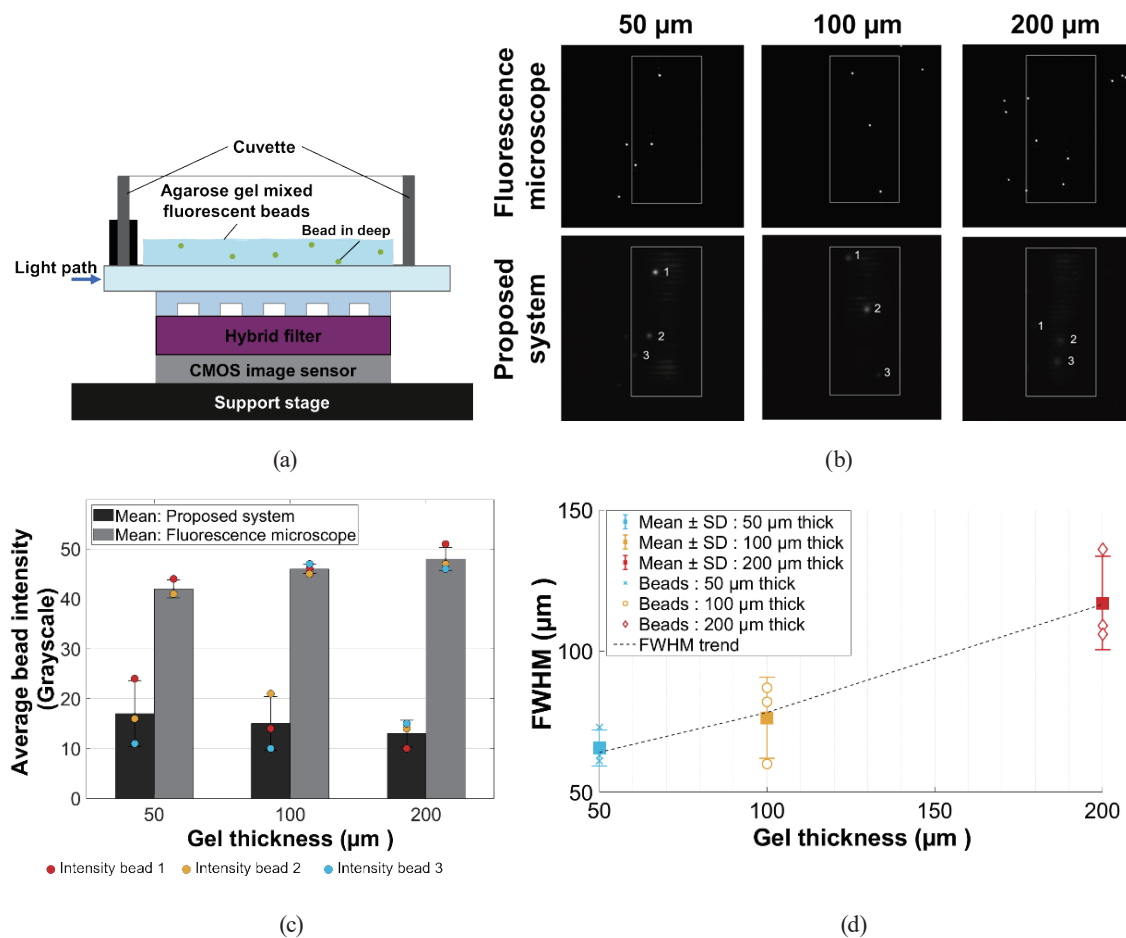


Fig. 9. (Color online) (a) Measurement system for brain tissue simulation using fluorescent beads embedded in agarose gels with thicknesses of 50, 100, and 200  $\mu\text{m}$ , (b) comparison of fluorescent bead emission within diffractor region between fluorescence microscope and our proposed system, (c) comparison of average intensity for each fluorescent bead within agarose gel layer, showing results from both fluorescence microscope and our proposed system along with mean values  $\pm$  s.d., and (d) results of FWHM analysis from our proposed system for each fluorescent bead within agarose gel layer in diffractor region, along with mean values  $\pm$  s.d.

system and a lower intensity in the fluorescence microscope, a trend most notable in the 100 and 200  $\mu\text{m}$  gel samples. These various intensities reflect the resolution of our system, which has the potential to detect the fluorescent target within the deep layers.

The predicted resolution of our system for detecting biological tissue is reflected in the FWHM data shown in Fig. 9(d). As light propagates through a thick agarose gel, scattering causes the fluorescent signal to broaden, making the beads appear larger and resulting in a higher mean FWHM. The mean FWHM was measured to be 65, 91, and 117  $\mu\text{m}$  for 50-, 100-, and 200- $\mu\text{m}$ -thick gels, respectively. For the 50- $\mu\text{m}$ -thick gel, the resolution was approximately 50  $\mu\text{m}$  larger than the actual bead size of 15  $\mu\text{m}$ , representing the highest resolution achieved in simulations of biological tissue experiments with our current proposed system.

#### 4. Discussion

The differences in the material properties of NOA 63, SU-8, and PDMS result in the diffractor's effectiveness. NOA 63, an acrylate-based resin containing photoinitiators, enables precise patterning and strong adhesion upon UV exposure. Similarly, SU-8, an epoxy-based resin, undergoes photo-crosslinking during UV curing. SU-8 provides excellent rigidity and high-resolution patterning. However, our experimental results indicate that its autofluorescence being higher than that of NOA 63 makes it less suitable for optical applications requiring low background noise. In contrast, PDMS, a silicone-based elastomer, cures via a crosslinking reaction at room temperature or higher. Despite its high optical transparency, its flexibility presents challenges in achieving uniform optical bonding, leading to uneven interfaces and multimode propagation in our study.

Therefore, we have proposed the effectiveness of NOA 63 as a diffractor in combination with a hybrid filter to enhance the quality of epi-fluorescence imaging in lensless image devices. Typically, the concept of the TIR confines excitation light within a waveguide and only excites fluorescence at the interface, which limits imaging depth in thick tissue. In our proposed system, the diffractor was designed to diffract excitation light into the hybrid filter layer, which then reflects the profile light toward the fluorescent sample. On the basis of this concept, we have demonstrated that our approach effectively excites fluorescent samples in deep layers of scattering media. Additionally, the use of linearly polarized light, maintained with PMF, coupled with our proposed front-light structure, has proven to be effective for enhancing the contrast image of fluorescent beads.

Despite its effectiveness, the current spatial resolution is still low. The hybrid filter and diffractor layer, which operate on a millimeter scale, increase the distance required to capture an image. In this study, we reduced the thickness of the light guide from 50 to 30  $\mu\text{m}$ , but the resolution was increased only about 10  $\mu\text{m}$ . Therefore, it is important to consider reducing the structure layer properties, such as the thickness of the hybrid filter layer,<sup>(24)</sup> and addressing specific technical needs, such as angle-selective pixels for miniature CMOS image sensors that can enhance spatial resolution.<sup>(25)</sup>

In addition to the significant distance, the stripe pattern image, combined with a target imaging of interest, tends to decrease in SNR. Although the NOA 63 diffractor is confirmed to be suitable for low-autofluorescence material and mechanical properties, the pattern image was still observed owing to the brightness of the diffractor region from excitation light, even with low exposure times. Considering low-fluorescence images, computational methods are required or NOA 81 (Norland Products Inc.) should be utilized, which is reported to have lower fluorescence levels than NOA 63.<sup>(26)</sup> Furthermore, given that PDMS demonstrates lower fluorescence levels than NOA materials, selecting an appropriate matching substrate is crucial for improving SNR.

An uneven excitation light distribution on the diffractor pattern is expected owing to optical losses caused by high reflection and refraction within the thickness of the diffractor. Additionally, effective control is needed to transfer a stripe pattern onto the glass. Although we can control the amount of NOA 63, the pressure applied to dispense a thin NOA 63 layer is

challenging, resulting in various diffractor dimensions, especially about  $\pm 3 \mu\text{m}$  of the base for every fabrication. Reducing the pattern thickness along with minimizing dimension variation, such as activating the vacuum to secure uniform contact, will increase the efficiency of the front-light structure.

As the fiber optic and glass were not fixed by adhesive, space is needed to avoid destroying a cross section of the core fiber during the switching of P- and S-polarized lights. Therefore, the transmission of light power and the excitation light intensity to irradiate a sample were slightly decreased. However, our final objective is to mount the front-light structure to the implantable image sensor device. The fiber optic and diffractor will be secured with adhesive, and we expect that the efficiency of light transmission will increase and the quality of the lensless images from our proposed system will be higher.

## 5. Conclusions

To address the low-contrast challenges in biological imaging for lensless devices, in this study, we proposed a high-performance front-light structure integrated with polarized excitation light to advance epifluorescence imaging in the lensless system. A low-fluorescence stripe diffractor, fabricated using NOA 63, was evaluated for its light-radiating performance compared with PDMS. The diffractor, designed to operate with a hybrid filter, was fabricated on a thin glass substrate to enhance light transmission efficiency. By implementing both P- and S-polarizations in the excitation light, the NOA 63 diffractor demonstrated a considerably improved emission of an excitation light profile directed toward the front of the image sensor. Specifically, S-polarized light exhibited a higher excitation intensity than P-polarized light, resulting in a more apparent contrast in fluorescent bead imaging. Furthermore, the proposed system successfully captured fluorescent signals across various agarose gel thicknesses, emphasizing its potential to detect low-fluorescence samples within deep layers of biological tissue.

## Acknowledgments

This study was supported by the Japan Society for the Promotion of Science KAKENHI (JP21H03809, JP23K21853, and JP23H05450), the Uehara Memorial Foundation, and the Murata Foundation.

## References

- 1 C. Han, S. Pang, D. V. Bower, P. Yiu, and C. Yang: *Anal. Chem.* **85** (2013) 2356. <https://doi.org/10.1021/ac303356v>
- 2 A. F. Coskun, I. Sencan, T.-W. Su, and A. Ozcan: *Opt. Express*. **18** (2010) 10510. <https://doi.org/10.1364/OE.18.010510>
- 3 S. Pang, C. Han, L. M. Lee, and C. Yang: *Lab Chip*. **11** (2011) 3698. <https://doi.org/10.1039/C1LC20654K>
- 4 S. A. Lee, X. Ou, J. Lee, and C. Yang: *Opt. Lett.* **38** (2013) 1817. <https://doi.org/10.1364/OL.38.001817>
- 5 X. Peng, X. Huang, K. Du, H. Liu, and L. Chen: *Biochem. Soc. Trans.* **47** (2019) 1635. <https://doi.org/10.1042/BST20190020>

- 6 T. Weidemann, J. Mücksch, and P. Schwill: *Curr. Opin. Struct. Biol.* **28** (2014) 69. <https://doi.org/10.1016/j.sbi.2014.07.008>
- 7 P. Nath, S. S. Hamadna, L. Karamchand, J. Foster, R. Kopelman, J. G. Amar, and A. Ray: *Analyst* **146** (2021) 3933. <https://doi.org/10.1039/D1AN00456E>
- 8 S. Khoubarfarin, E. K. Dadson, and A. Ray: *Photonics* **11** (2024) 575. <https://doi.org/10.3390/photonics11060575>
- 9 J. Wu, Y. Chen, A. Veeraraghavan, E. Seidemann, and J. T. Robinson: *Nat. Commun.* **15** (2024) 1271. <https://doi.org/10.1038/s41467-024-45417-6>
- 10 J. K. Adams, D. Yan, J. Wu, V. Boominathan, S. Gao, A. V. Rodriguez, S. Kim, J. Carns, R. Richards-Kortum, C. Kemere, A. Veeraraghavan, and J. T. Robinson: *Nat. Biomed. Eng.* **6** (2022) 617. <https://doi.org/10.1038/s41551-022-00851-z>
- 11 J. Ohta, Y. Ohta, H. Takehara, T. Noda, K. Sasagawa, T. Tokuda, M. Haruta, T. Kobayashi, Y. M. Akay, and M. Akay: *Proc. IEEE*. **105** (2017) 158. <https://doi.org/10.1109/JPROC.2016.2585585>
- 12 Y. Sunaga, H. Yamaura, M. Haruta, T. Yamaguchi, M. Motoyama, Y. Ohta, H. Takehara, T. Noda, K. Sasagawa, T. Tokuda, Y. Yoshimura, and J. Ohta: *Jpn. J. Appl. Phys.* **55** (2016) 03DF02. <https://doi.org/10.7567/JJAP.55.03DF02>
- 13 Y. Dattner and O. Yadid-Pecht: *Sensors* **10** (2010) 5014. <https://doi.org/10.3390/s100505014>
- 14 H. Takehara, Y. Ohta, M. Motoyama, M. Haruta, M. Nagasaki, H. Takehara, T. Noda, K. Sasagawa, T. Tokuda, and J. Ohta: *Biomed. Opt. Express.* **6** (2015) 1553. <https://doi.org/10.1364/BOE.6.001553>
- 15 R. R. Singh, D. Ho, A. Nilchi, G. Gulak, P. Yau, and R. Genov: *IEEE Trans. Circuits Syst. I Regul. Pap.* **57** (2010) 1029. <https://doi.org/10.1109/TCSI.2010.2043990>
- 16 M. I. Azmer, K. Sasagawa, E. Rustami, K. Sugie, Y. Ohta, M. Haruta, H. Takehara, H. Tashiro, and J. Ohta: *Jpn. J. Appl. Phys.* **60** (2021) SBBG07. <https://doi.org/10.35848/1347-4065/abe5bf>
- 17 C. Richard, A. Renaudin, V. Aimez, and P. Charette: *Lab Chip.* **9** (2009) 1371. <https://doi.org/10.1039/b819080a>
- 18 K. Sasagawa, Y. Ohta, M. Kawahara, M. Haruta, T. Tokuda, and J. Ohta: *AIP Adv.* **9** (2019) 035108. <https://doi.org/10.1063/1.5083152>
- 19 K. Sasagawa, A. Kimura, M. Haruta, T. Noda, T. Tokuda, and J. Ohta: *Biomed. Opt. Express.* **9** (2018) 4329. <https://doi.org/10.1364/BOE.9.004329>
- 20 K. Sasagawa, Y. Ito, D. Schaeffer, Y. Sunaga, H. Takehara, M. Haruta, H. Tashiro, and J. Ohta: *Proc. IEEE BioCAS* (2023) 1. <https://doi.org/10.1109/BioCAS58349.2023.10389024>
- 21 K. Ren, J. Zhou, and H. Wu: *Acc. Chem. Res.* **46** (2013) 2396. <https://doi.org/10.1021/ar300314s>
- 22 J. H. Sim, H. J. Moon, Y. H. Roh, H. W. Jung, and K. W. Bong: *Korean J. Chem. Eng.* **34** (2017) 1495. <https://doi.org/10.1007/s11814-017-0041-1>
- 23 T. Turcitu, C. J. K. Armstrong, N. Lee-Yow, M. Salame, A. V. Le, and M. Fenech: *Micromachines* **14** (2023) 2033. <https://doi.org/10.3390/mi14112033>
- 24 E. Rustami, K. Sasagawa, K. Sugie, Y. Ohta, H. Takehara, M. Haruta, H. Tashiro, and J. Ohta: *Sensors* **23** (2023) 3695. <https://doi.org/10.3390/s23073695>
- 25 K. Sugie, K. Sasagawa, M. C. Guinto, M. Haruta, T. Tokuda, and J. Ohta: *Electron. Lett.* **55** (2019) 729. <https://doi.org/10.1049/el.2019.1031>
- 26 P. Wägli, A. Homsy, B. Guélat, and N. F. de Rooij: *MicroTAS* (2010) 3.

## About the Authors



**Arphorn Promking** received her B.S. degree in electrical engineering from Ubon Ratchathani University, Thailand, in 2019 and her M.S. degree in electrical engineering from Chulalongkorn University, Thailand, in 2021. She is currently pursuing her Ph.D. degree at Nara Institute of Science and Technology. Her research interests include lensless CMOS imaging devices and bioimaging. ([promking.arphorn.pd0@naist.ac.jp](mailto:promking.arphorn.pd0@naist.ac.jp))



**Yoshinori Sunaga** received his B.E. degree from Chiba University, Japan, in 2012 and his M.E. and Ph.D. degrees from the Graduate School of Materials Science, Nara Institute of Science and Technology (NAIST), Japan, in 2014 and 2017, respectively. In 2017, he joined NAIST as a postdoctoral fellow and began collaborative research between NAIST and the University of Houston. In 2019, he joined the University of Houston as a postdoctoral fellow. He joined NAIST as a postdoctoral fellow in 2022 and was specially appointed as an assistant professor in 2023. He is interested in developing novel devices for observing and assessing animal brain activity to reveal new brain mechanisms. ([sunaga.yoshinori@ms.naist.jp](mailto:sunaga.yoshinori@ms.naist.jp)).



**Yasumi Ohta** received her B.S. degree in physics from Nara Women's University in 1984. She enrolled in the Faculty of Science at Kyoto University in 2004 and switched to a master's program at the Graduate School of Science, Kyoto University, in 2006. She received her M.S. and Ph.D. degrees in biophysics from Kyoto University, Kyoto, Japan, in 2008 and 2011, respectively. From 1984 to 1986, she worked at Mitsubishi Electric Corp. in Hyogo, Japan. In 2011, she joined Nara Institute of Science and Technology (NAIST) in Nara, Japan, as a postdoctoral fellow. Her research interests include implantable bioimaging CMOS sensors and neuroscience. ([ohtay@ms.naist.jp](mailto:ohtay@ms.naist.jp)).



**Ryoma Okada** received his B.E. degree in electrical and electronic engineering from Shizuoka University, Shizuoka, Japan, and his M.E. and Ph.D. degrees from Nara Institute of Science and Technology (NAIST), Japan, in 2022 and 2024, respectively. Recently, he has been appointed as an assistant professor at NAIST. His current research interests include polarization image sensors and electromagnetic field imaging ([okada.ryoma.on9@ms.naist.jp](mailto:okada.ryoma.on9@ms.naist.jp)).



**Hironari Takehara** received his M.E. degree in applied chemistry from Kansai University in 1986 and his Ph.D. degree from Nara Institute of Science and Technology (NAIST) in 2015. From 1986 to 2012, he worked as a semiconductor process engineer at Panasonic Corporation in Kyoto, Japan, where he was involved in developing BiCMOS, high-voltage SOI, and optoelectronic IC processes. He then joined NAIST, where he conducted research on image sensors, bioimaging, and optical filters, and served as an assistant professor from 2019 to 2024. He is currently the CEO of Nara Advanced Imaging Technology, Co., Ltd., a NAIST-certified startup, where he continues his work in imaging technology. ([t-hironari@ms.naist.jp](mailto:t-hironari@ms.naist.jp)).



**Makito Haruta** received his B.E. degree in bioscience and biotechnology from Okayama University, Okayama, Japan, in 2009 and his M.S. degree in biological science and Dr. Eng. degree in material science from Nara Institute of Science and Technology (NAIST), Nara, Japan, in 2011 and 2014, respectively. He was a postdoctoral fellow with NAIST from 2014 to 2016. He joined the Institute for Research Initiatives, NAIST, in 2016, as an assistant professor. In 2019, he joined the Graduate School of Science and Technology, NAIST, as an assistant professor and became an associate professor at Chitose Institute of Science and Technology, Hokkaido, Japan, in 2023. His research interests include brain imaging devices for understanding brain functions related to animal behaviors. ([m-haruta@ms.naist.jp](mailto:m-haruta@ms.naist.jp)).



**Hiroyuki Tashiro** received his B.E. and M.E. degrees in electrical and electronic engineering from Toyohashi University of Technology (TUT), Aichi, Japan, in 1994 and 1996, respectively. He received his Ph.D. degree in engineering from Nara Institute of Science and Technology (NAIST), Nara, Japan, in 2017. In 1998, he joined Nidek Co., Ltd., Aichi, Japan, where he worked on the research and development of ophthalmic surgical systems and retinal prostheses. In 2004, he joined the Faculty of Medical Sciences, Kyushu University, Fukuoka, Japan, as an assistant professor, and since 2019, he has also been an adjunct associate professor at NAIST. His current research interests include artificial vision systems and neural interfaces. ([tashiro.hiroyuki.289@m.kyushu-u.ac.jp](mailto:tashiro.hiroyuki.289@m.kyushu-u.ac.jp)).



**Jun Ohta** received his B.E., M.E., and Dr. Eng. degrees in applied physics from The University of Tokyo, Japan, in 1981, 1983, and 1992, respectively. In 1983, he joined Mitsubishi Electric Corporation, Hyogo, Japan. From 1992 to 1993, he was a visiting scientist at the Optoelectronics Computing Systems Center at the University of Colorado, Boulder. In 1998, he joined the Graduate School of Materials Science, Nara Institute of Science and Technology (NAIST), Nara, Japan, as an associate professor, and he was appointed as a professor in 2004. His current research interests include smart CMOS image sensors for biomedical applications and retinal prosthetic devices. He is a Fellow of IEEE, the Japan Society of Applied Physics, and the Institute of Image, Information, and Television Engineers. ([ohta@ms.naist.jp](mailto:ohta@ms.naist.jp))



**Kiyotaka Sasagawa** received his B.S. degree from Kyoto University in 1999 and his M.E. and Ph.D. degrees in materials science from NAIST, Japan, in 2001 and 2004, respectively. Subsequently, he became a researcher at the National Institute of Information and Communications Technology in Tokyo, Japan. In 2008, he joined NAIST as an assistant professor and became an associate professor in 2024. Last year, he was promoted to professor. His research interests include bioimaging, biosensing, and electromagnetic field imaging. ([sasagawa@ms.naist.jp](mailto:sasagawa@ms.naist.jp))